Vol. 92 No. 1 pp. 225–240 ACTA GEOLOGICA SINICA (English Edition) Feb. 2018

Zircon U-Pb age, Trace Element, and Hf Isotopic Compositions of Nordmarkite in the Lizhuang Rare Earth Element Deposit in the Western Margin of the Yangtze Block

ZHOU Jiayun*, TAN Hongqi, GONG Daxin, ZHU Zhimin and LUO Liping

Institute of Multipurpose Utilization of Mineral Resources, Chinese Academy of Geological Sciences, Chengdu, 610041

Abstract: The Mianning–Dechang (MD) rare earth element (REE) belt, located in the northern Kangdian axis (KDA) in the western margin of the Yangtze platform, is one of the most economically significant REE mineral belts in China. REE mineralization is associated with Himalayan carbonatite–alkaline complexes. The Lizhuang nordmarkite occurred in the northern part of the MD REE belt. The majority of zircons from the Lizhuang nordmarkite are characterized by pronounced positive Ce yet slightly negative Eu anomalies and high U/Yb. Moreover, all zircons have stable Hf isotopic compositions with initial $^{176}Hf/^{177}Hf$ ratios ranging from 0.282739 to 0.282808 and an average value of 0.282773. The negative Lu/Hf and positive $\varepsilon_{Hf}(t)$ range from −0.98 to −0.94 (average value of −0.96) and from −0.56 to 1.89 (the majority is positive, with an average of 0.66), respectively. These characteristics indicate that the rock is derived from an enriched mantle and subducted material. LA-ICP-MS analysis of the zircons from the intrusion yields a weighted mean $^{206}Pb/^{238}U$ age of 28.57±0.61Ma. During this period, the tectonic activity in the KDA is not plate subduction but an intraplate tectonic exhibiting fold–thrust and strike–slip behaviors in the western marginal zone of the Yangtze platform (WMYB). We suggest the possibility of an existing eastward old slab subduction under WMYB combined with a regional tectonic evolution. The Lizhuang nordmarkite may be derived from an enriched mantle beneath the western part of the Yangtze craton, which originated from the remelting of the Tethys subducting slab, because of the Himalayan strike–slip that formed a special type of REE deposit called strike–slip-type REE deposits.

Key words: nordmarkite, REE deposit, Hf isotopic characteristics of zircon, Lizhuang

1 Introduction

The Himalayan Mianning-Dechang (MD) rare earth element (REE) belt in Western Sichuan Province, Southwestern China, which is one of the most economically significant REE mineral belts in China, is 270 km long and 15 km wide, and is one of the three large rare earth production bases hosting one giant (Maoniuping), one large (Dalucao), two small and medium-sized (Muluozhai and Lizhuang), and numerous small REE deposits (Tian Shihong et al., 2008). In the belt, REE mineralization is associated with Himalayan carbonatite–alkaline complexes (Hou Zengqian et al., 2008; Hou et al., 2009), and thus the tectonic setting, evolution, and REE mineralization have caught the attention of many scholars. Most carbonatite–alkalic complexes and their hosting REE deposits usually occur in continental rift zones (Mitchell et al., 1981). Their origin is commonly considered to be related to mantle plume activity and interpreted as a result of the interaction between the HIMU mantle plume and the EM Ⅰ lithosphere mantle (Bell et al., 1996). However, the MD REE belt occurs in the eastern Indian–Asian collision zone, which is controlled by large-scale strike–slip faults and tensional fissure zones (Fig.1, Hou Zengqian et al., 2008). Previous studies reported inconsistent ages between alkaline magmatism syenite formation and REE mineralization (40–10 Ma; Yuan Zhongxing et al., 1995; Pu Guangping, 2001; Tian Shihong et al., 2008). This outcome indicates that these carbonatite–alkaline complexes and REE deposits formed during Himalayan orogenesis, thus suggesting the formation to be during collisional orogenesis rather than during continental rifting (Liu et al., 2015). Furthermore, Wang Denghong et al.

* Corresponding author. E-mail: zhszjy@aliyun.com

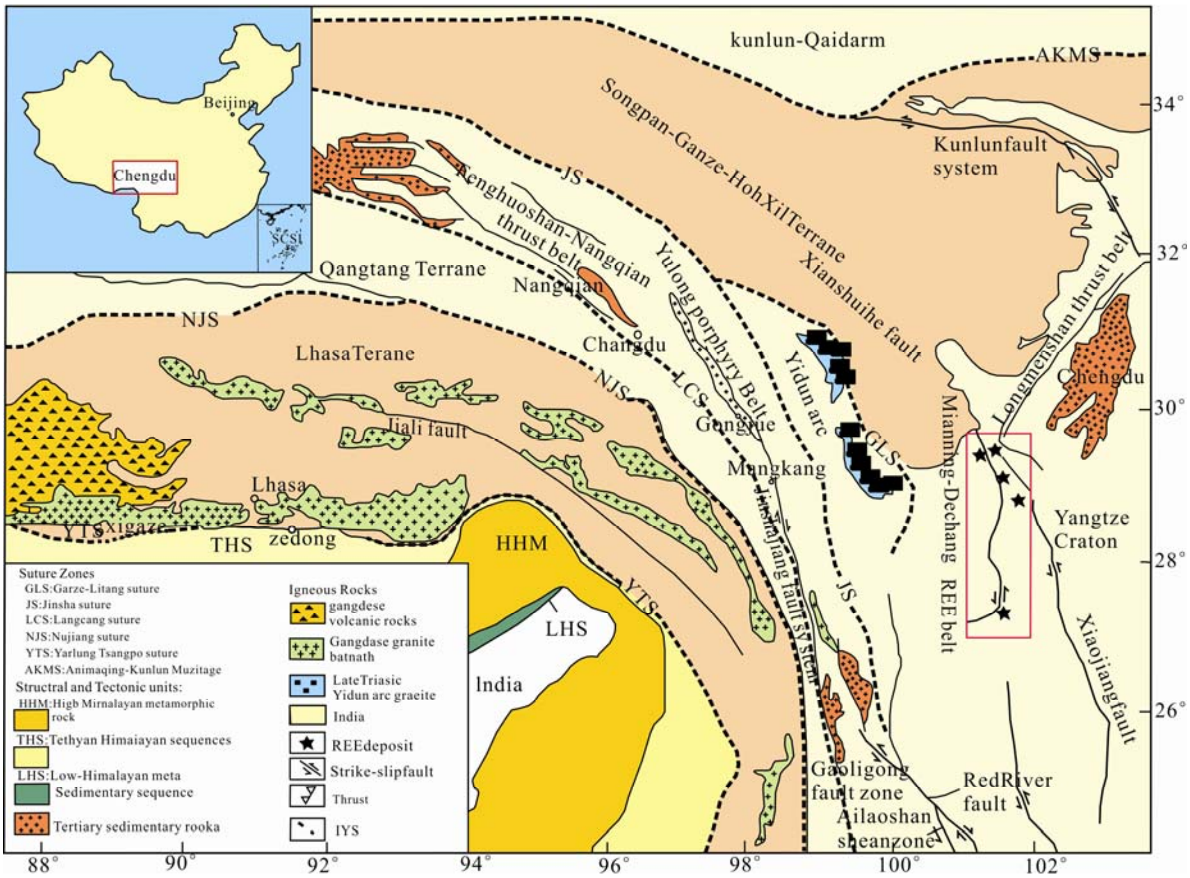

Fig. 1. Simplified tectonic map of the Himalayan–Tibetan orogen (modified from Liu et al., 2015).

(2001) considered the Maoniuping deposit as a special "orogenic–type" REE deposit. This finding indicates that the origin and timing of the carbonatite–syenite complex are important to constraining the type of mineralization in this giant REE belt.

Previous studies have used a number of differing analytical techniques, such as geochemistry, dating (K-Ar), and isotope systems (Sr and Pb) for the host rock, to identify the genesis of syenite (Wang Denghong et al., 2002; Xu Cheng et al., 2002, Zhou Jiayun et al., 2007; Xu et al., 2008). However, the geochemical and isotopic data on the rocks themselves offer little help to the detailed genetic arguments because such data provide only a picture of the end result without a record of the progress. Fortunately, the fine-scale zoning of many zircon crystals in magmatic rocks preserves this record (Griffin et al., 2002). Despite its small size, the emplacement of host rock and REE mineralization of the Lizhuang REE deposit occur in the deepest place in the REE belt (Hou Zengqian et al., 2008), and it is an important role in the study of magma evolution and mineralization as well as a good material for the study of the continental dynamics background in REE mineralization. In this paper, we report the U-Pb dating and isotopic composition of Hf and trace-element character in the zircon population obtained by *in-situ* analysis with a laser-ablation microprobe coupled to a multi-collector ICPMS. These data allow for a robust test of the hypothesis and dating of the host rock and provide mineralogical and petrological evidence for the metallogenic model of orogenic-type REE formations in the MD Himalaya period.

2 Geological Setting

2.1 Regional geology

The MD REE belt is located in the northern Kangdian axis (KDA) in WMYP (Figs. 1). The KDA underwent a complicated tectonic evolution from Proterozoic lithospheric accretion through the Paleozoic–Mesozoic continental margin, followed by a Cenozoic collision orogeny (Zhang Yunxiang et al., 1988; Yu Anguang et al., 1998). Specifically, it formed the Panxi rift under extensional tectonic activities in the Hercynian–Indosinian period (Miao Yikun et al., 1986) and the Jinpingshan mountain under intracontinental convergence in the Yanshan–Himalaya period, which is characterized by a double structure of earlier opening and later closing (Xu Zhiqin et al., 2007).

The regional stratigraphy in the KDA can be divided into two tectonic unites: basement rocks and overlying sedimentary rocks (Miao Yikun, 1986). The basement consists of Archaean high-grade metamorphic rocks and Proterozoic meta-sedimentary rocks, and the sedimentary comprises Phanerozoic clastic and carbonate sequences (Cong Bolin, 1988; Luo Yaonan et al., 1998; Hou et al., 2009). Following the strong tectonic activity, the KDA underwent frequent magmatism. Especially in the Hercynian, the large-scale basic–ultrabasic magmatism, which comprised the well-known Emei flood basalt in China associated with vanadium titano-magnetite, marked large intrusion-related deposit. The Himalayan carbonatite–alkaline complexes are associated with REE mineralization, which consists of carbonatitic sills or dykes, and alkaline syenite stocks, and characterized by the model of some small intrusions forming large deposits. The carbonatite–alkaline complexes mainly intruded a Proterozoic crystalline basement and an overlying Paleozoic–Mesozoic volcano-sedimentary sequence and constituted a narrow, NS-tending REE-bearing belt. The belt is bordered by NS-striking strike–slip faults, and individual complexes with irregular shapes are controlled by second-order strike–slip faults or transtensional faults (Hou et al., 2009).

2.2 Ore deposit geology

The Lizhuang deposit, a small-sized REE deposit with grades of 1.05%–6.69% REO is located in the Western Mianning County, where a Yanshanian alkali–feldspar granite and a Himalayan carbonatite–alkalic complex intruded an N1000 m-thick sequence of Silurian–Triassic lower greenschist facies clastic rocks and carbonates (Hou et al., 2009). The Lizhuang complex is associated with REE mineralization, which consists of NNW-striking carbonatite sills and a nordmarkite body. The carbonatite mainly consists of calcite and subordinate aegirine–augite (Hou et al., 2009). The main phase of the associate stock is nordmarkite, which is about 100 m wide and 400 m long (Fig. 2). The nordmarkite is a gray, massive structure with a fine-grained texture. It is mainly been made up of perthite (70%–75%), aegirine–augite (about 12%), quartz (about 10%), and minor accessory minerals composed of subordinately albite, arfvedsonite, hematite, rarely titanite, apatite, pyrite, barite, and fluorite (Fig. 3a). A small amount of albite and quartz is contained in Perthite, which shows a myrmekitic texture (Fig. 3b). Previous studies used Ar–Ar isotope systems to date the host rocks, yielding an age of 27.1 Ma (Tian Shihong et al., 2008).

Fenitization is the main alteration associated with mineralization, and it is characterized by the replacement of plagioclase by alkali feldspar and the occurrence of aegirine, aegirine–augite, arfvedsonite, episodite, and biotite. This alteration produces a fenitization halo around

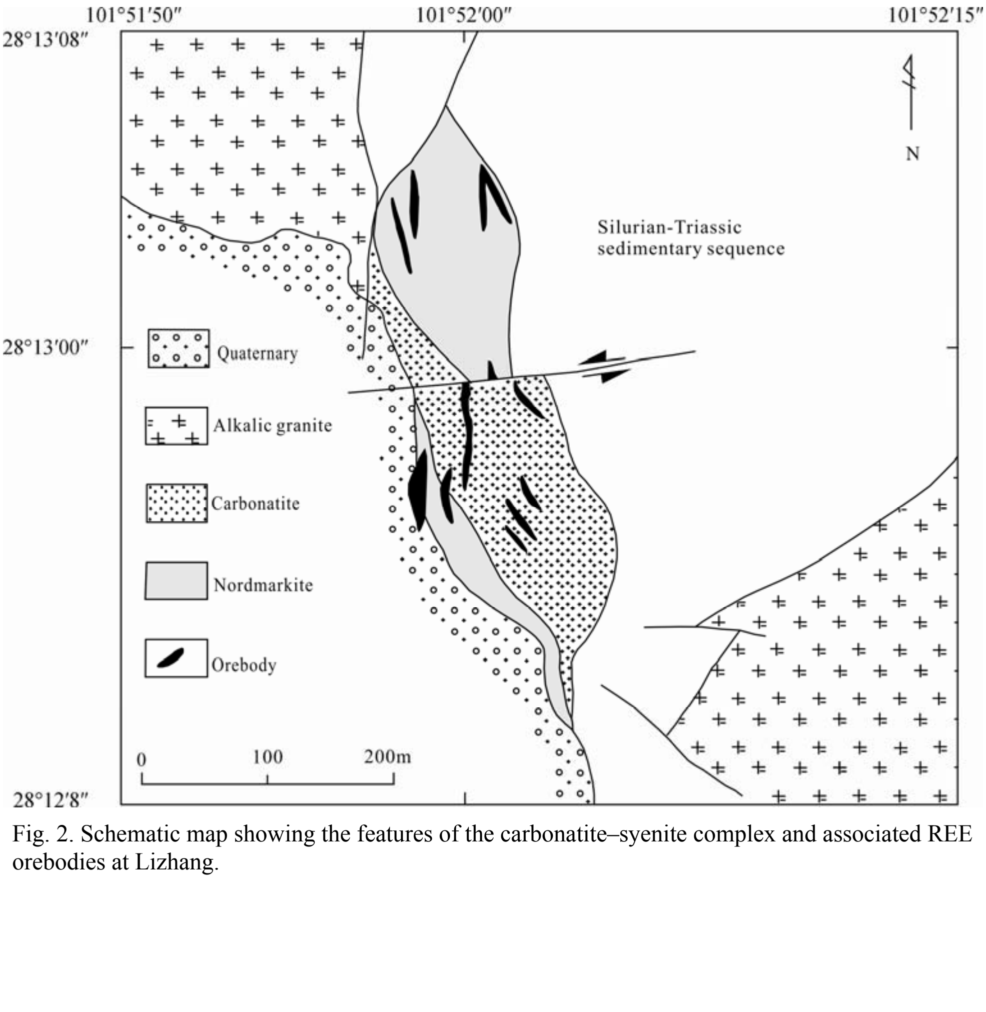

Fig. 2. Schematic map showing the features of the carbonatite–syenite complex and associated REE orebodies at Lizhang.

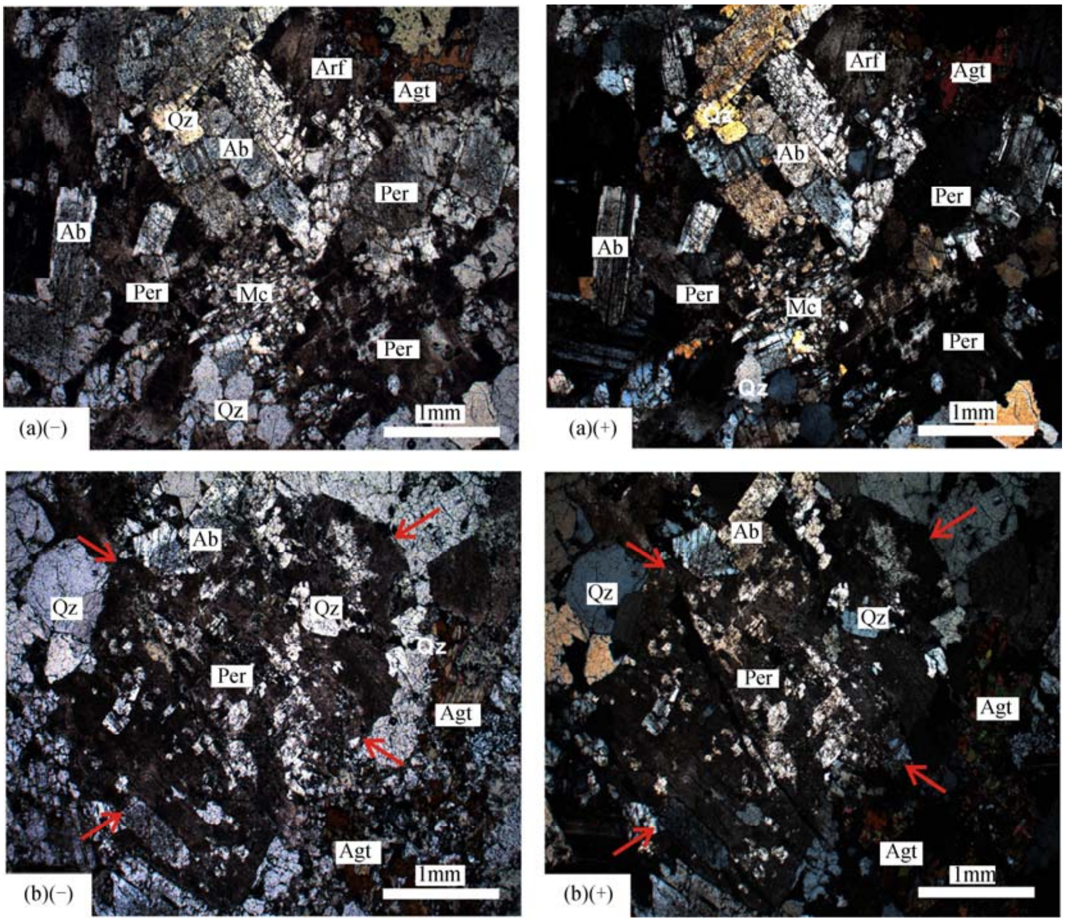

Fig. 3. Photomicrograph showing the texture of the Lizhuang nordmarkite.
(a), Mineral composition; (b), myrmekitic texture of Perthite.

the carbonatite–alkalic complex. The Lizhuang deposit consists of a number of small lenses and stockwork ores hosted in the carbonatite sills and nordmarkite stocks. These orebodies are 30–100 m in length and 2.2–11.6 m thick, and they were developed along fissure zones within the carbonatite sills (Fig. 2). Four types of ores have been recognized. Brown disseminated ore is dominant and consists of calcite (53%–59%), fluorite (20%–25%), barite (10%–16%), and minor bastnaesite (3%–6%), occurring as lent or veinlet. Yellow banded ore, the second significant type, mainly occurs as lent, and it consists of an assemblage of calcite (58%), barite (12%), fluorite (10%), bastnaesite (12%), and minor biotite and quartz. Stockwork ore mainly occurs in the nordmarkite stock, which is composed of fine veins containing fluorite + bastnaesite + barite assemblages. Black powder-like ore, consisting of aegirine–augite and bastnaesite, sporadically occurs in ore lenses or fissures in carbonatite sills. In general, mineral associations at Lizhuang are relatively simple, and the paragenesis is comparable with those in the Maoniuping and Dalucao deposits (Hou et al., 2009). The difference in Lizhuang is that vein ore mainly developed along the X-type fracture within complex rock, which occurs as lent or veinlet, thus forming a large number of small lenses and disseminated ores, which are different from the pegmatoid ore at Maoniuping and the brecciated ore at Dalucao. These deviations indicate that REE mineralization occurred in a relatively deep environment (Hou Zengqian et al., 2008).

Previous studies used a number of different analytical techniques, isotope systems, and minerals to date the Lizhang deposit and determine the REE metallogenic age (30.55 Ma, Ar–Ar on biotite; 28.5 Ma, model age, Re–Os on molybdenite) (Tian Shihong et al., 2008).

3 Sampling and Analytical Methods

3.1 Zircon U-Pb dating and Hf isotopic analyses

The samples (called LZ) for the zircon LA-ICP-MS U-Pb dating, Hf isotope, and trace element analyses were selected from nordmarkites in the open pit of the Lizhuang REE deposit. The pit is located at 28°13′12″N lat and 101°52′24″E long. Zircon grains were separated from nordmarkites samples using the conventional heavy liquid and magnetic techniques and then by handpicking under a binocular microscope at the Langfang Geological Survey in Hebei Province, China. The individual crystals were mounted in epoxy resin, polished to reveal the cross-section of the grains, and then photographed in both reflected and transmitted light according to the method of Song Biao (2002). After the grain interiors were exposed for the cathodoluminescence (CL) and backscatter imaging, the sites were selected for further analysis. The CL and BSE imaging, U-Pb dating, Hf isotope, and trace element analyses of zircon were conducted at the MRL key laboratory of Metallogeny and Mineral Assessment, Institute of Mineral Resources, Chinese Academy of Geological Sciences, Beijing.

U-Pb isotopic and trace element analyses of zircon were simultaneously performed by Newwave UP 213 laser-ablation systems coupled with a Bruker M90 MC-ICP-MS. The 213 nm ArF excimer laser, homogenized by a set of beam delivery groups, was focused on the zircon surface with energy density of 2.5 J/cm^2. The ablation protocol employed a spot diameter of 25 μm at a 10 Hz repetition rate for at least 30 s. More detailed instrumental setting and analytical procedures were described by Hou Kejun et al. (2009). In the zircon U-Pb analysis, Zircon GJ1 and Plesovice were used as the external standard for U-Pb dating and examined twice for every four analyses. Off-line raw data selection, integration of background and analytical signals, and time–drift correction and quantitative calibration for U-Pb dating were performed by ICPMS Data 8.0 (Liu et al., 2008). Measured compositions were corrected for common Pb using non-radiogenic ^{204}Pb (Andersen, 2002). Concordia diagrams, binned frequency histograms, and weighted mean ages were generated using Isoplot 3.0 (Ludwig, 2003), and the results were reported with 1σ errors. For further data interpretation, the detailed analysis procedure and principle similar to those in Hou Kejun et al. (2009) were adopted.

After the zircon U-Pb analyses, Hf isotope analysis was conducted on zircon grains in situ using the Newwave UP213 laser-ablation system attached to a Neptune MC-ICP-MS. A stationary spot, with a beam diameter of 55 μm and a repetition rate of 10 Hz, was used for the present analysis. In the analysis, helium was used as the carrier gas. To correct the isobaric interferences of ^{176}Lu and ^{176}Yb on ^{176}Hf, ^{176}Lu/^{175}Lu=0.02655 and ^{176}Yb/^{172}Yb=0.5886 ratios were determined (Xie Liewen et al., 2008). International standard GJ1 zircon samples were used as reference. The weighted average of ^{176}Hf/^{177}Hf of the GJ1 zircon samples was 0.282008±0.000013 (n=11, 2σ), consistent with the values (0.282015±0.000019, using LA-ICP-MS) reported in the literature (Elhlou et al., 2006). Details of the instrumental conditions and test process were given in Hou Kejun (2007).

Zircon trace element concentration results were simultaneously obtained during zircon U-Pb dating. Combined with external standard GJ1, ^{29}Si was used as an internal standard to correct the trace element concentrations of the unknowns. A detailed calibration procedure for each element was presented in Wu Yuanbao et al. (2004b). The average analytical error ranged from 15% for light REEs to 5% for other trace elements. The raw data calibrated by ICPMS DataCal 8.0 and associated calculation are shown in Table 3.

4 Analytical Results

4.1 Zircon morphology

The external morphology of zircon combined with its internal structure has the ability to record magma evolution histories (Helena et al., 2014). Zircon grains from the Lizhuang nordmarkite are subhedral–euhedral, colorless, and transparent, with short columnar, graininess, and double prismatic shapes. They have a length of 120–150 μm, width of 80–100 μm, and length/width ratio of 3:2. The crystal face remains intact, and the crystal size is comparatively uniform. The study conducted by BSE and CL reveals that most grains (Nos. 1, 4, 6, 8, 11, 13, 14, 15, 16, 18, 22, 23, 24, and 26) are dark to slightly bright, thus revealing obvious oscillatory zoning (Fig. 4a) with a rare nebulitic structure. Oscillatory zoning is comparatively wide, which indicates that the zircons crystallized at a high temperature (Zhou Jianxiong et al., 2007). The nebulitic structure is characterized by a diffused structure, which is prevalent in less evolved zircons (Helena et al., 2014). Other grains (Nos. 3, 5, 7, 9, 10, 17, and 21) reveal a wide magmatic zoning with small bright cores (Fig. 4b), which show a distinct core–rim structure that indicates an inherited zircon core caught from an early source rock. Other zircons (Nos. 2, 12, 20, 25, 28, 29, and 30) develop thin overgrowths following the grain boundary (Fig. 4c).

4.2 U-Pb dating of zircon

A total of 23 analyses were conducted on 28 zircon crystals, which were separated from the nordmarkite sample LZ. Fourteen of the analyses were obtained from the integrated zoning zircon, seven from the inherited core zircon, and seven from the overgrowth zircon. All spots analyses were performed in magmatic zoning domains (Fig. 4, Table 1), and they were mostly in accordance with the apparent ^{206}Pb/^{238}U age of 25.78–31.16 Ma. However, six data points from the inherited core zircon and three data points from the overgrowth zircon were excluded because of relatively low analytical concordance in ^{206}Pb/^{238}U and ^{207}Pb/^{206}Pb rations, thus suggesting Pb loss

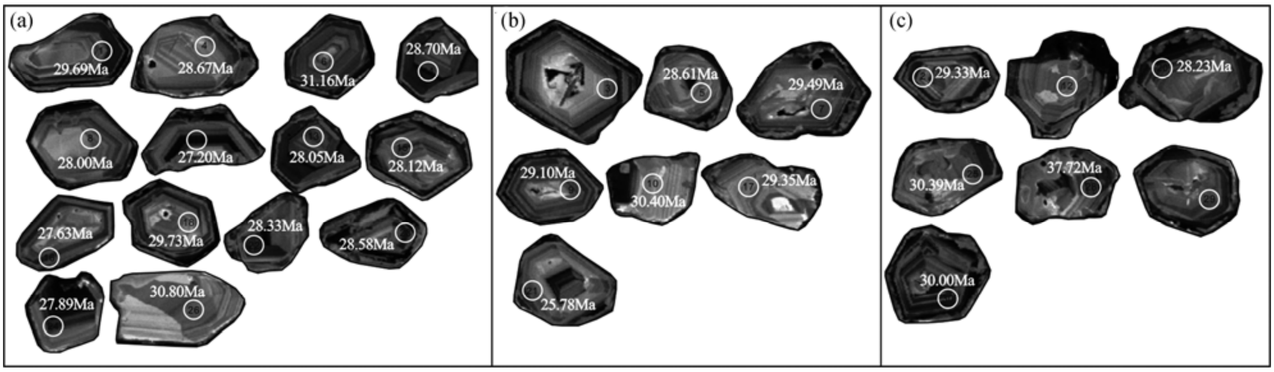

Fig. 4. CL images of zircon from the Lizhuang nordmarkite.
(a), Integrated zoning zircons; (b), inherited core zircons; (c), overgrowth zircons.

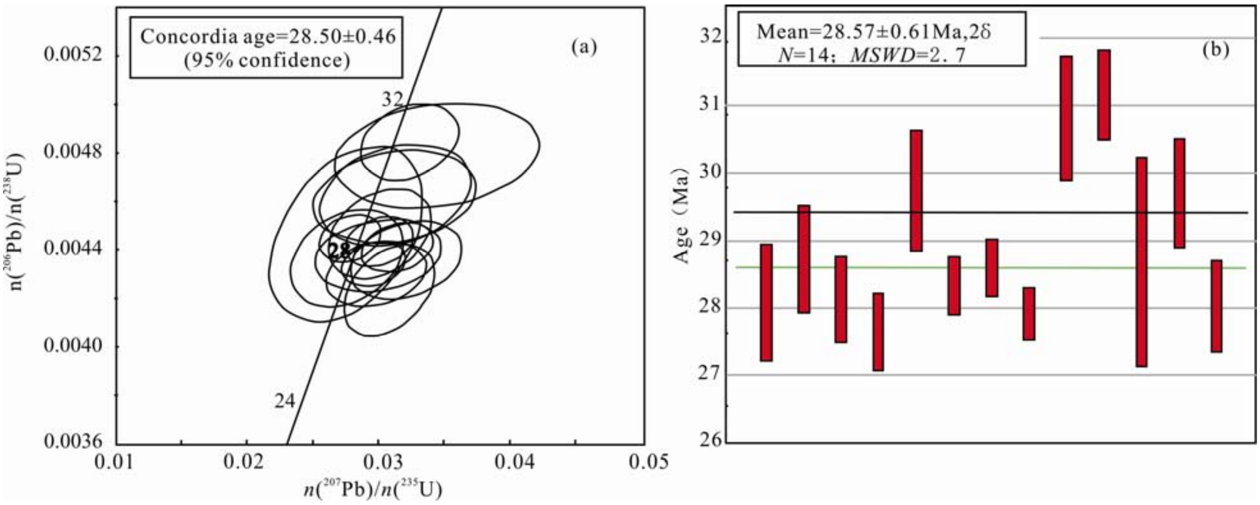

Fig. 5. Zircon U-Pb concordia diagram and weighted average dating of the Lizhuang nordmarkite
(a), Zircon U-Pb concordia diagram; (b), weighted average age.

during the process of partial recrystallization or late thermal events. The U-Pb data for the integrated zoning zircon are plotted in Fig. 5, and the consequence of the zircons with small ^{207}Pb is presented in the concordia plot in Fig. 5a. Fourteen analytical points with high U (1663.11–19937.06 ppm) and Th (1564.46–2405231.32 ppm) content and Th/U (0.63–120.64) ration yielded a concordant age (28.50±0.46 Ma) within error. The $^{206}Pb/^{238}U$ age is 27.20–31.16 Ma with a weighted mean of 28.57±0.61 Ma and MSWD=2.7, which is well interpreted to date zircon crystallization during Himalayan period (Fig. 5b).

4.3 Lu-Hf isotopic characteristics of zircon

In situ Hf isotopic analyses of zircons from Lizhuang nordmarkites samples (LZ) are shown in Table 2, and the zircon Hf zircon isotopic data and calculation results are presented in Table 2. Twenty spot analyses were obtained from 20 grains. In general, the $^{176}Lu/^{177}Hf$ ratios of magmatic domains are <0.002, with an average of 0.0012774. This result indicates that time-integrated changes to the $^{176}Hf/^{177}Hf$ ratio as a result of the in situ decay of ^{176}Lu proceed at virtually negligible rates (Kinny, 2003；Yin et al., 2015). Therefore, zircon effectively preserves the initial $^{176}Hf/^{177}Hf$ ratio, providing an enduring record of the Hf isotopic composition of its source environment at the time of crystallization. According to the average crystal components ($^{176}Lu/^{177}Hf$=0.008, Taylor and McLennan, 1985) and zircon U-Pb age (28.57±0.61 Ma) to calculate the Hf isotopic model, $\varepsilon_{Hf}(t)$ values, and T_{DM2}, the data show that the magmatic zircons from Lizhuang nordmarkites (28.57±0.61 Ma) have stable Hf isotopic compositions, with initial $^{176}Hf/^{177}Hf$ ratios ranging from 0.282739 to 0.282808 and an average value of 0.282773. The negative Lu/Hf and positive $\varepsilon_{Hf}(t)$ ranges from −0.98 to −0.94 (average value of −0.96) and from −0.56 to 1.89 (the majority is positive with an average of 0.66). The corresponding T_{DM2} age varies from 989 Ma to 1145 Ma, with an average of 1067 Ma, which indicates that the nordmarkite originates from enriched mantle formed in the Middle Proterozoic.

Table 1 LA-ICP-MS U-Pb isotopic analytical data of zircon in Lizhuang nordmarkite

No.	Element (ppm)			Th/U	Isotope ratio						Apparent age (Ma)					
	Pb^{*}	Th	U		$^{207}Pb/^{206}Pb$	1σ	$^{207}Pb/^{235}U$	1σ	$^{206}Pb/^{238}U$	1σ	$^{207}Pb/^{206}Pb$	1σ	$^{207}Pb/^{235}U$	1σ	$^{206}Pb/^{238}U$	1σ
integrated zoning zircon																
1	2991	2405231	19937	120.64	0.0501	0.0062	0.0313	0.0041	0.0046	0.0501	211.19	26.66	31.25	4.03	29.69	0.82
4	612	525234	7618	68.94	0.0467	0.0083	0.0275	0.0038	0.0045	0.0002	31.58	377.73	27.58	3.78	28.67	1.56
6	1060	762424	13515	56.41	0.0485	0.0037	0.0324	0.0025	0.0048	0.0001	120.46	174.05	32.33	2.44	31.16	0.67
8	756	567506	9066	62.59	0.0550	0.0051	0.0321	0.0028	0.0044	0.0001	413.01	208.15	32.10	2.76	28.00	1.05
11	2097	1641204	17384	94.41	0.0546	0.0047	0.0308	0.0023	0.0042	0.0001	398.2	199.05	30.82	2.25	27.20	0.80
13	782	660733	9340	70.74	0.0476	0.0053	0.0276	0.0028	0.0044	0.0001	79.72	244.41	27.65	2.78	28.05	0.86
14	926	706218	11942	59.13	0.0489	0.0040	0.0301	0.0026	0.0045	0.0001	142.68	181.45	30.11	2.53	28.70	0.80
15	387	301631	4647	64.91	0.0506	0.0057	0.0300	0.0032	0.0044	0.0001	220.44	244.42	30.01	3.13	28.12	0.63
16	790	692542	5933	116.71	0.0508	0.0046	0.0298	0.0025	0.0043	0.0001	231.55	212.94	29.81	2.49	27.63	0.57
18	159	131409	1906	68.93	0.0507	0.0068	0.0313	0.0038	0.0046	0.0001	227.85	294.42	31.29	3.75	29.73	0.90
22	23	2797	4475	0.63	0.0517	0.0031	0.0314	0.0018	0.0044	0.0001	272.29	167.57	31.43	1.79	28.33	0.44
23	9	1564	1663	0.94	0.0461	0.0027	0.0278	0.0015	0.0044	0.0001	400.05	261.07	27.86	1.51	28.58	0.42
24	25	4334	4063	1.07	0.0495	0.0026	0.0296	0.0016	0.0043	0.0001	168.6	128.69	29.66	1.59	27.89	0.39
26	4	693	802	0.86	0.0547	0.0090	0.0345	0.0051	0.0048	0.0001	398.2	329.59	34.39	5.02	30.80	0.92
inherited core zircon																
3	1389	1114757	14209	78.45	—	—	—	—	—	—	—	—	—	—	—	—
5	869	651313	7631	85.35	0.0550	0.0073	0.0348	0.0051	0.0045	0.0002	409.31	299.96	34.75	4.99	28.61	1.27
7	1034	553499	7727	71.63	0.1017	0.0082	0.0629	0.0048	0.0046	0.0001	1655.2	150.16	61.91	4.59	29.49	0.67
9	1916	1457019	11512	126.56	0.085	0.0070	0.0528	0.0044	0.0045	0.0001	1316.6	159.26	52.21	4.25	29.10	0.77
10	455	339220	3634	93.33	0.0884	0.0083	0.0539	0.0041	0.0047	0.0002	1391.6	147.38	53.35	3.97	30.40	1.14
17	138	131823	1895	69.55	0.0674	0.0165	0.0406	0.0098	0.0046	0.0003	849.99	530.52	40.40	9.56	29.35	1.61
21	23	2021	3667	0.55	0.0511	0.0035	0.0280	0.0017	0.0040	0.0001	242.66	157.39	28.02	1.68	25.78	0.32
overgrowth zircon																
2	1410	1089538	13735	79.32	0.0644	0.0126	0.0385	0.0062	0.0046	0.0004	753.71	422.19	38.33	6.04	29.33	2.54
12	845	414825	4258	97.42	—	—	—	—	—	—	—	—	—	—	—	—
20	43	30277	946	31.98	0.0700	0.0111	0.0414	0.0067	0.0044	0.0001	929.32	330.07	41.21	6.53	28.23	0.87
25	4	645	579	1.11	0.1161	0.0095	0.0690	0.0047	0.0047	0.0001	1898.1	147.07	67.79	4.50	30.39	0.94
28	9	793	958	0.83	—	—	—	—	—	—	—	—	—	—	37.72	—
29	33	4468	3447	1.30	—	—	—	—	—	—	—	—	—	—	—	—
30	18	2758	2947	0.94	—	—	—	—	—	—	—	—	—	—	31.0	—

Table 2 Hf isotopic compositions of zircon in Lizhuang nordmarkite

spot	$^{176}Hf/^{177}Hf$	2σ	$^{176}Yb/^{177}Hf$	2σ	$^{176}Lu/^{177}Hf$	2σ	$\varepsilon_{Hf}(0)$	$\varepsilon_{Hf}(t)$	T_{DM1} (Ma)	T_{DM2} (Ma)	$f_{Lu/Hf}$
LZ-01	0.282757	0.000015	0.039502	0.000219	0.001163	0.000005	−0.53	0.10	704	1103	−0.96
LZ-02	0.282757	0.000015	0.039502	0.000219	0.001163	0.000005	−0.55	0.07	705	1104	−0.96
LZ-04	0.282802	0.000014	0.039475	0.000096	0.001148	0.000001	1.07	1.68	640	1001	−0.97
LZ-05	0.282800	0.000013	0.033176	0.000214	0.001018	0.000009	1.01	1.61	640	1006	−0.97
LZ-06	0.282761	0.000013	0.031427	0.000238	0.000910	0.000009	−0.39	0.28	694	1093	−0.97
LZ-07	0.282767	0.000011	0.027289	0.000228	0.000799	0.000004	−0.17	0.46	683	1080	−0.98
LZ-08	0.282767	0.000014	0.040752	0.000740	0.001167	0.000017	−0.18	0.41	690	1082	−0.96
LZ-11	0.282769	0.000016	0.043010	0.000822	0.001226	0.000021	−0.11	0.46	689	1078	−0.96
LZ-13	0.282744	0.000015	0.066253	0.000466	0.001914	0.000007	−0.99	−0.41	738	1135	−0.94
LZ-14	0.282801	0.000013	0.043318	0.000194	0.001262	0.000008	1.03	1.63	644	1005	−0.96
LZ-15	0.282789	0.000015	0.040362	0.000441	0.001255	0.000015	0.59	1.19	661	1033	−0.96
LZ-16	0.282753	0.000012	0.037046	0.000492	0.001073	0.000015	−0.67	−0.08	708	1113	−0.97
LZ-18	0.282765	0.000014	0.060358	0.001091	0.001611	0.000027	−0.25	0.36	702	1087	−0.95
LZ-20	0.282768	0.000014	0.038309	0.000129	0.001109	0.000004	−0.14	0.45	688	1080	−0.97
LZ-22	0.282739	0.000013	0.040332	0.000404	0.001140	0.000013	−1.16	−0.56	729	1145	−0.97
LZ-23	0.282798	0.000018	0.064544	0.001434	0.002003	0.000053	0.93	1.52	660	1011	−0.94
LZ-24	0.282781	0.000013	0.041886	0.000228	0.001208	0.000006	0.31	0.90	672	1051	−0.96
LZ-25	0.282808	0.000014	0.073832	0.000302	0.001926	0.000007	1.26	1.89	646	989	−0.94
LZ-26	0.282768	0.000017	0.034404	0.000126	0.000937	0.000003	−0.15	0.50	685	1079	−0.97
LZ-30	0.282772	0.000015	0.058656	0.000304	0.001516	0.000007	0.01	0.66	689	1069	−0.95

4.4 Trace element composition of zircon

Zircon trace element concentration results were simultaneously obtained during zircon U-Pb dating. Combined with external standard GJ1 and SRM, some erratic high content was rejected. The raw data calibrated by ICPMS Data 8.0 and associated calculation are listed in Table 3. The chondrite-normalized REE patterns are shown in Fig. 6. The zircons measured in this study have variable concentrations of ΣREE, ranging from 1118 ppm to 6659.21 ppm. All trace element data show HREE-enriched REE patterns related to LREE, with low ΣCe/ΣY ratio (0.13−0.33), and marking left sloping pattern of REE distributions; this finding indicates that the differentiation degree of the magma is high (Ma Yanping et al., 2007). Therefore, two groups of zircons can be distinguished on the basis of the Eu and Ce anomalies. These integrated oscillatory zoning zircons and overgrowth rim zircons have a pronounced positive Ce but slightly negative Eu anomalies. Alternatively, the inherited core zircons are characterized by slightly

Table 3 Trace element analysis of zircon from the Lizhuang nordmarkite

spot	Ti	Nb	La	Ce	Pr	Nd	Sm	Eu	Gd	Tb	Dy	Ho	Er	Tm	Yb	Lu	Y	Hf	Ta	ΣREE	LREE/HREE	δEu	δCe
	ω(B) (ppm)																						
integrated zoning zircon																							
LZ-01	4.07	17.59	0.10	531.05	1.60	12.86	20.84	31.33	195.23	54.50	431.01	121.57	530.69	101.67	862.45	163.10	4021.82	20387.74	2.48	3057.98	0.24	0.99	92.87
LZ-04	1.15	9.35	0.01	191.01	0.16	3.45	9.06	9.80	58.21	18.15	177.38	55.99	270.32	54.76	537.35	95.98	1923.28	21164.37	1.53	1481.65	0.17	0.98	322.56
LZ-06	2.12	16.34	0.06	154.83	0.31	3.74	6.54	9.89	62.90	19.46	175.78	57.44	309.25	66.34	639.28	129.75	2181.44	23904.23	2.28	1635.58	0.12	0.97	131.04
LZ-08	3.26	25.23	0.08	243.22	0.34	7.72	11.50	18.64	95.32	30.22	287.81	95.17	459.98	96.08	865.56	156.12	3280.03	19866.25	2.40	2367.78	0.13	1.19	185.81
LZ-15	1.76	21.39	4.35	112.78	0.52	6.01	32.69	19.04	129.50	56.50	390.02	122.26	649.79	54.53	1106.51	2095.33	4237.20	22091.72	3.02	4779.84	0.04	0.78	15.08
LZ-18	1.58	11.01	8.38	55.96	0.33	5.58	28.59	14.95	44.11	17.80	118.93	35.82	202.47	15.81	336.83	632.39	1427.31	20333.40	2.13	1517.93	0.08	1.28	4.64
LZ-22	1.41	51.89	0.31	419.70	0.36	5.03	47.46	16.52	136.33	42.21	387.55	145.84	813.62	159.86	816.23	292.16	5631.68	28093.01	5.57	3283.19	0.18	0.58	252.94
LZ-23	1.39	14.57	0.04	326.90	0.34	4.84	42.92	16.72	128.09	33.08	251.43	81.53	410.29	74.79	368.92	139.77	2790.54	23579.13	3.00	1879.66	0.26	0.64	268.13
LZ-24	2.22	48.71	0.02	813.28	0.63	12.35	102.62	32.86	231.77	60.91	497.55	159.21	797.66	143.86	654.14	231.67	5516.28	22253.84	8.12	3738.54	0.35	0.63	366.10
LZ-26	1.56	14.45	0.02	238.90	0.17	4.49	31.43	11.75	78.19	25.30	197.13	67.99	353.68	62.77	314.79	112.53	2247.63	20972.41	2.68	1499.14	0.24	0.69	374.74
inherited core zircon																							
LZ-03	1.06	15.05	0.72	270.69	2.02	14.70	17.46	23.18	140.71	43.29	363.29	115.30	534.78	104.64	969.89	171.19	3825.38	22627.56	2.67	2771.85	0.13	1.00	33.89
LZ-05	1.50	12.38	0.02	259.77	0.60	6.95	14.21	17.50	98.19	30.05	256.27	74.31	355.21	70.60	609.06	108.20	2592.17	20773.92	1.57	1900.93	0.19	1.05	123.20
LZ-07	3.16	15.76	1.78	229.89	3.85	24.10	16.38	20.58	103.12	30.88	262.48	84.29	391.66	78.53	692.84	125.71	2785.32	21231.69	2.02	2066.09	0.17	1.16	14.58
LZ-09	1.45	21.31	0.46	259.12	1.35	12.29	15.26	18.82	88.29	26.01	242.25	73.99	363.33	73.76	677.50	124.30	2700.43	20389.13	1.92	1976.71	0.18	1.22	48.76
LZ-10	2.06	7.61	0.05	243.10	0.24	7.58	10.00	15.67	51.19	14.64	132.26	39.73	190.64	36.73	319.51	56.66	1372.31	16983.94	1.72	1118.00	0.33	1.71	275.61
LZ-21	2.71	62.32	0.95	613.22	1.39	12.03	79.05	25.94	180.02	47.97	388.24	130.56	646.19	114.25	553.07	196.25	4447.69	22060.66	6.95	2989.15	0.32	0.64	100.67
overgrowth zircon																							
LZ-02	1.03	25.32	0.01	376.04	0.53	2.55	15.50	16.33	110.76	37.34	323.03	104.39	554.43	119.67	1005.15	199.51	3977.38	20616.60	2.65	2865.25	0.17	0.87	201.37
LZ-25	3.48	13.86	10.60	697.35	11.10	48.64	76.38	26.87	140.57	38.12	304.86	99.46	503.90	89.58	419.29	150.07	3292.99	17116.26	2.99	2616.78	0.50	0.78	13.26
LZ-28	1.80	14.35	17.57	544.09	16.84	66.13	107.65	28.96	138.65	35.96	265.04	86.10	423.54	76.62	365.09	124.16	2813.44	24119.28	4.42	2296.42	0.52	0.72	6.66
LZ-29	1.40	66.40	7.39	660.83	2.81	14.42	89.36	33.28	270.21	82.78	746.52	263.87	1409.62	264.86	1279.56	419.45	9653.88	24027.77	6.83	5544.97	0.17	0.60	33.96
LZ-30	1.35	31.58	47.76	1225.57	41.05	153.30	179.38	40.32	227.57	57.87	462.74	160.90	847.45	156.87	783.66	279.84	5533.79	23966.24	5.21	4664.26	1687.37	2976.89	0.57

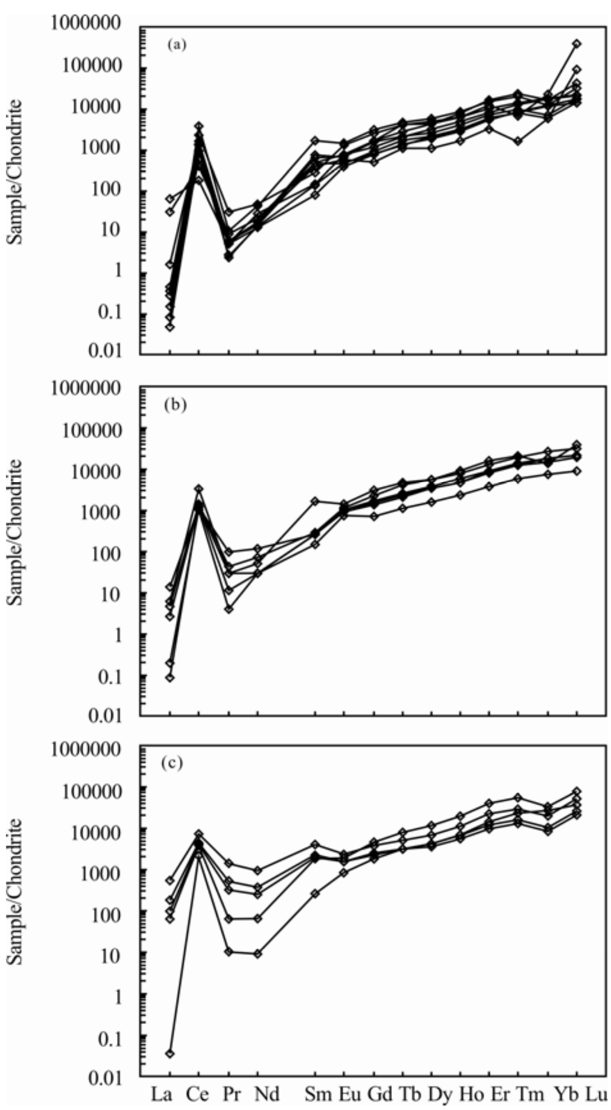

Fig. 6. Chondrite-normalized REE patterns in zircons from Lizhuang nordmarkite(normalization values after Taylor and McLennan, 1985).
(a), Integrated zoning zircons; (b), inherited core zircons; (c), overgrowth zircons.

positive Eu anomalies, with the positive Ce not being far off. In brief, the REE patterns show the characteristics of mantle magmatic zircon (Lei Weiyan et al., 2013).

5 Discussion

5.1 Zircon-type discrimination

Zircons with different origins have different sizes, growth morphologies, and internal structures, which can be distinguished in the CL images (Li et al., 2014). Magmatic zircons are commonly hypidiomorphic–idiomorphic crystals, have a grain size of 20–250 μm, and exhibit a pronounced internal zoning (Hoskin and Schaltegger, 2003; Yuan et al., 2015). Conversely, hydrothermal zircons have no or have a weak zoning phenomenon (Li et al., 2014) and usually have a special internal texture, such as cloud, facial, and taxitic zoning (Wu Yuanbao et al., 2004a). Zircon grains from the Lizhuang nordmarkite are hypidiomorphic–idiomorphic, colorless, and transparent, with short columnar graininess and double prismatic shapes. They have a length of 120–150 μm, which indicates that these zircons have a magmatic origin.

Unaltered magmatic zircons usually show steep heavily enriched REE patterns that rise rapidly from Sm to Lu, thus marking positive Ce and negative Eu anomalies (Belousova et al, 2002; Hoskin and Schaltegger, 2003; Fu et al., 2009; Lei Weiyan et al., 2013). The REE compositions of zircons in this study are generally typical for igneous zircons, that is, they are highly enriched in the heaviest REE. Specifically, these zircons show integrated zoning and overgrowth, are characterized by pronounced Ce but a slight negative Eu anomaly, and are different from hydrothermal zircon (Fu et al., 2009), thus indicating their magmatic origin (Figs. 6a, 6c and Fig. 7a). The Th/U ratios are also used as an indicator of zircon types (Li et al., 2014). Magmatic zircons usually have high Th and U contents, and their Th/U ratios are composed of hydrothermal zircon (Hoskin et al., 2000). Th/U ratios $>$ 0.4 is a hint of magmatic origin, and Th/U ratios $<$0.1 is a hint of hydrothermal origin. For the Lizhuang nordmarkite, all zircons have Th/U ratios greater than 0.4 (Fig. 7b), which definitely implies a magmatic origin. Further distinction between hydrothermal and magmatic zircons can be identified from the discriminant diagrams proposed by Hoskin (2005). In Fig. 7c, most data from the integrated zoning zircons and inherited core zircons fall within or near the field of magmatic zircons, which have high $(Sm/La)_N$ values (12.02–7561.50) and low La values (0.01–4.35). Overgrowth zircons have low $(Sm/La)_N$ values (6.01–19.38) and high La values (7.39–47.76), and fall outside the typical range of magmatic zircons, thus suggesting a trend toward hydrothermal compositions. In Fig. 7d, the integrated zoning zircons and inherited core zircons are characterized by a prominent positive Ce anomaly ranging from 15.08 to 374.74 and 14.72 to 1008.51, respectively, with most of the data plotted within or near to the magmatic field. However, the overgrowth zircons are more inclined to be plotted than the hydrothermal zircons, with the Ce/Ce^* values ranging from 0.57 to 33.96. This finding suggests the existence of a transitional composition between magmatic and hydrothermal zircons (Fig. 7d).

Furthermore, magmatic zircons are more likely to have higher Nb/Ta and Hf/Y ratios than hydrothermal zircons (Pettke et al, 2005). For the zircons in the Lizhuang nordmarkite, the integrated zoning zircons and inherited core zircons contain higher Nb/Ta and Hf/Y ratios than the overgrowth zircons (Figs. 7e-f), possibly suggesting a magmatic origin, but the overgrowth zircons could undertake fluid transformation processes (Li et al., 2014). In a word, the zircons coming from the Lizhuang nordmarkite still belong to a magmatic origin, but a few grains could have been weakly undertaken during the fluid transformation processes.

5.2 Zircon source rocks

Different trace element profiles of zircons qualitatively reflect the evolution and chemical variation of their parent magma. Zircon crystals contain a record of multiple geologic events (Li et al., 2014), and thus zircon studies play an important role in distinguishing the origin of igneous rocks (Nardi et al., 2012).

Previous studies pointed out the significantly different REE patterns between mantle zircons and crustal zircons. Mantle-affinity zircons have positive Ce anomalies and slightly negative or no significant Eu anomalies (Belousova et al., 1998), but crust-affinity zircons always have pronounced positive Ce anomalies and negative Eu anomalies (Ce-enriched yet Eu-depleted REE patterns) (Belousova et al., 1998; Li et al., 2000; Hoskin et al., 2000). The magnitude of the Eu anomaly increases with the increase in fractionation (Claiborne et al., 2010). In this study, the most magmatic zircons are considered positive Ce and slightly negative Eu anomalies, thus indicating their mantle-derived magma origin and slight fractionation of the magma.

Hf, U, and Th are important trace elements for defining the source and evolution of magma. They are common in zircons but less in most silicate minerals. Belousova (2002) found a good correlation between the trace element patterns of zircon and the composition of its magmatic host rock. Classification and regression trees were developed for classifying a set of objects based on the multivariate measurements of the characteristics of each object (Belousova et al., 2002). In the Lizhuang nordmarkite, zircons contain 56.66–2095.33 ppm Lu, which indicates that the rock from which the zircons are derived is Ne–Syenite or Syenite Pegmatites (Fig. 8a). The zircons also have high average U (6766 ppm), Ta (343 ppm), and Hf concentrations (2.17%), and Ce/Ce^* values (136.5), which indicate that these zircons crystallized from Larvikite (Fig. 8b). Grimes (2007) pointed out that plots of U/Yb ratio versus Hf and Y show distinct fields for zircons crystallized in ocean gabbros, continental granitoids, and kimberlites. Average U/Yb ratios for zircons from different settings are disparate and increase from ocean gabbros (0.18) to continental granitoid (1.07) and then to kimberlites (2.1). In this study, the magmatic

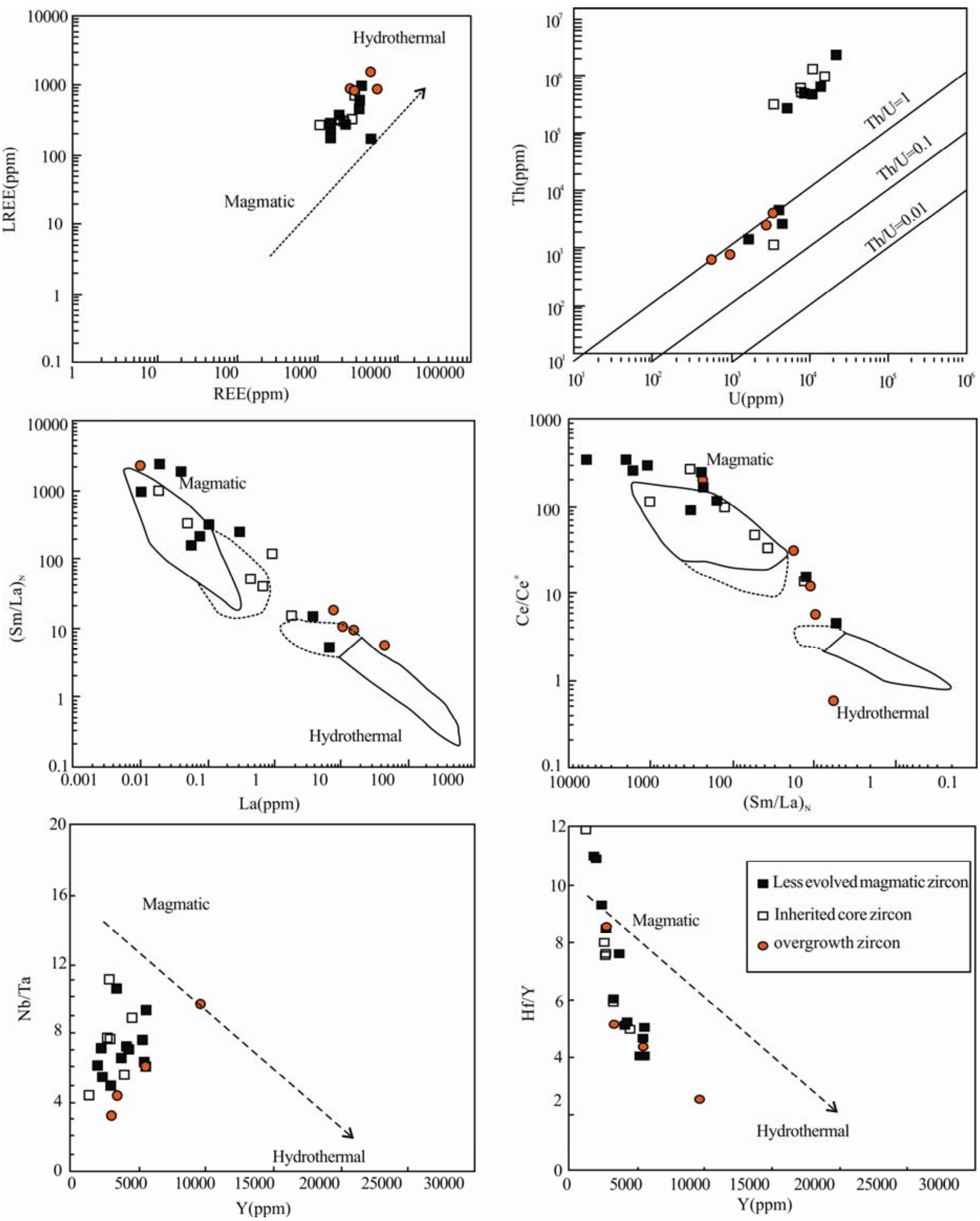

Fig. 7. Discriminant diagrams of some trance element for the zircons from Lizhuang nordmarkite (Li et al., 2014).
(a), ΣREE vs. LREE; (b) U vs. Th; (c) La vs. $(Sm/La)_N$; (d) $(Sm/La)_N$ vs.Ce/Ce^*; (e) Y vs. Nb/Ta ; (f) Y vs. Hf/Y.

zircon U/Yb ratios vary from 2.55 to 23.12 at an average of 10.17. The high U/Yb ratios >4 are probably inherited from enriching mantle-sourced host magmas. Specifically, in the discrimination diagrams of U/Yb ratio versus Hf (Fig. 9a) and Y (Fig. 9b), the zircons recovered from the Lizhuang nordmarkite were predominately plotted in the field of modern continental zircon.

The zircon Lu-Hf isotope analysis is also an important method for tracing the geochemical origin of rocks. In the study of Hf isotopes, the Hf isotopic composition of some important geochemical reservoirs is the basis for discussion. The presence of such enriched (low Lu/Hf)

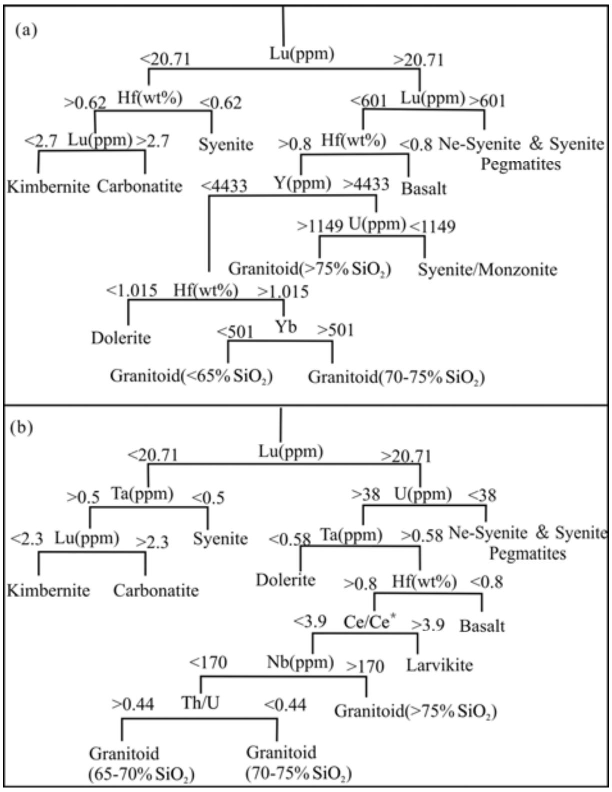

Fig. 8. Classification trees based on the trace element composition of zircon (Belousova et al., 2002).
(a), Short classification trees; (b), long classification trees.

reservoirs in the low crust was demonstrated by the highly negative $\varepsilon_{Hf}(t)$ values of −12 and −10 (Peter et al., 2003). Depleted (high Lu/Hf) mantle was a detected source for magmatic rocks, so that rocks yielded $\varepsilon_{Hf}(t)$ values up to +14 (present-day oceanic basalts have $\varepsilon_{Hf}(t)$ up to +23) (Peter et al., 2003). Studies on zircon Hf isotopes of the Lizhuang nordmarkite found that the $\varepsilon_{Hf}(t)$ values vary from −0.41 to 1.89. The average value is 0.66, which is near to 0, significantly different from that of the depleted mantle and crust. The nordmarkite rocks appear to be composed not only of depleted mantle but also of continental crust by Hf isotopes. In the zircon T-$\varepsilon_{Hf}(t)$ diagram, the data are predominately plotted near the evolution line of the chondrite (Fig. 10). Previous studies proposed that the $\varepsilon_{Hf}(t)$ values of zircons were close to zero and interpreted to represent the primary mantle source that coexisted spatially and temporally with the depleted mantle. However, an alternative possibility is the contamination of magma from a depleted mantle source with old crust carrying an enriched Hf signature (Peter et al., 2003). However, in the Lizhuang nordmarkite, evidence against the two processes abounds. First, the xenoliths and xenocrysts caught from older basement rocks have not been found in the nordmarkite, thus implying that the Lizhuang nordmarkite may not be contaminated by the crust. Second, the zircon model age (1067 Ma) is clearly older than the forming age (28.57 Ma), which initially indicates that the primitive mantle-like isotope signatures in nordmarkite are unlikely the result of the rock coming from the primitive mantle, as the uncontaminated igneous rocks that come from the CHUR reservoir or depleted mantle sources often show a consistency between the model age and the forming age (Chen Jun et al., 2004). Therefore, current research has confirmed that the enriched mantle is another potential source for Hf enriched, with highly negative $\varepsilon_{Hf}(t)$ values (down to −16) (Peter et al., 2003). Therefore, we can infer that $\varepsilon_{Hf}(t)$ values that are close to zero are also interpreted to represent the enriched mantle source that coexists with the depleted mantle. The $^{177}Hf/^{176}Hf$ values of zircon sampled from Lizhuang nordmarkite vary at 0.282739–0.282808, with an average value of 0.282773, which significantly deviates from the $^{177}Hf/^{176}Hf$ values of the depleted mantle (0.2831–0.2835) but is near those of EMⅠenriched mantle (0.2826–0.2827) and EMⅡenriched mantle (0.2828) (Zhang Benren et al., 2005). Previous studies also showed that the Lizhuang nordmarkite have an extremely high $(^{87}Sr/^{86}Sr)_i$ of 0.706578–0.706925 and a relative low $(^{143}Nd/^{144}Nd)_i$ of 0.512390–0.512423 as well as a wide range of $^{208}Pb/^{204}Pb$ (38.403–38.557), $^{206}Pb/^{204}Pb$ rations (18.211–18.295), and $^{207}Pb/^{204}Pb$ rations (15.602–15.618), which are different

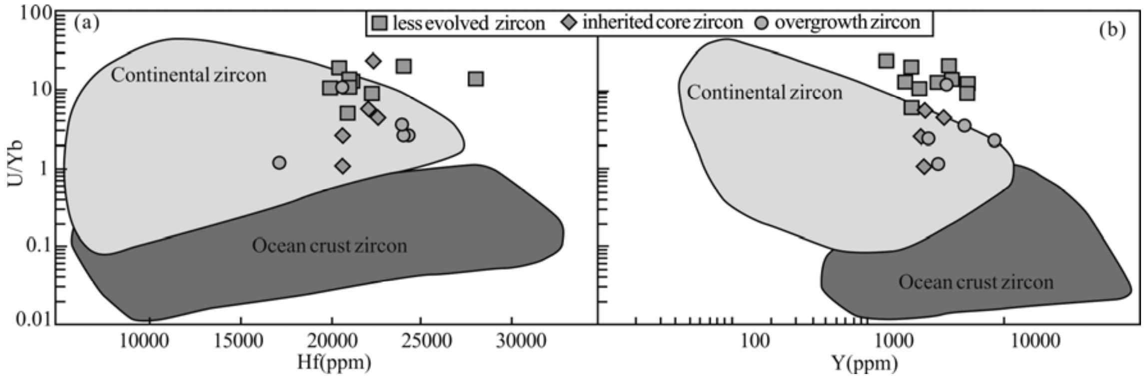

Fig. 9. Discrimination diagrams of U/Yb ratio versus Hf and Y (modified from Grimes et al., 2007).
(a), U/Yb ratio versus Hf; (b), U/Yb ratio versus Y.

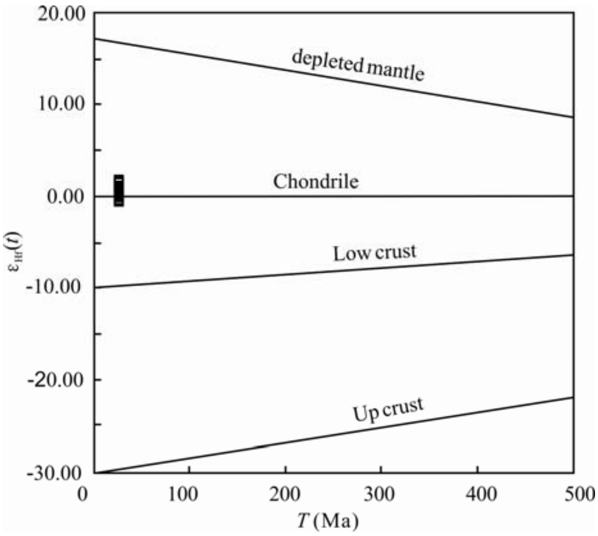

Fig. 10. Zircon t-$\varepsilon_{Hf}(t)$ diagram of the Lizhuang nordmarkite (modified from Griffin et al, 2002; Yu et al., 2011).

from most depleted mantle rocks around the world and but similar to EMI or EMII components (Tian Shihong, 2005). Therefore, the whole characteristics of zircons indicate the host rocks were derived from an enriched mantle.

5.3 Genesis of a fertile mantle source

Subduction and delamination are the main modalities of recycling the lithosphere to form an enriched mantle (Chen Jun et al., 2004). Previous studies found that the Lizhang nordmarkite is characterized by enriched lithophile elements and high-field-strength elements and depleting transitional elements, such as Nb, Ta, Zr, Hf, and Ti. It exhibits remarkably negative Ti, Nb, and Ta anomalies in the primitive mantle-normalized trace element diagram, thus indicating that the intrusion probably formed in a subduction setting (Tian Shihong, 2005). Based on this viewpoint, some scholars (Wang Denghong et al., 2002; Xu Cheng et al., 2002) connected the REE mineralization with the subduction.

LA-ICP-MS analysis of zircons from the intrusion yields a weighted mean $^{206}Pb/^{238}U$ age of 28.57±0.61 Ma, which confirms that the intrusion formed in Himalayan period. However, during the Himalayan period**,** the western part of the Yangtze craton had experienced intracontinental deformation since the middle-late Triassic, and no further oceanic plate subduction had occurred beneath the western part of the craton (Wang et al., 2000). The eastern Indo–Asian collision zone has several suture zones marked as Yarlung Tsangpo suture, Nujiang suture (NJS), Langcang suture (LCS), Jinsha suture, and Ganzi-Litang suture (GLS) from the west toward the east; and the GLS is regarded as the western boundary of the Yangtze craton (Guo et al., 2005). Traditionally, this area is considered an adjustment for absorbing the deformation caused by the Indo–Asian collision in the Himalayan period (Yan Quanren et al., 2006), in which a multi-level slip and rise (Hou Zengqian et al., 2006) with a large-scale strike–slip occurred and the syntaxes were clearly and decisively analyzed (Yin et al., 2000; Zhang Yueqiao et al., 2004; Xu Zhiqin et al., 2016). Therefore, the Himalayan tectonic activity in KDA is not a straightforward plate subduction between plates but rather a mid-plate tectonic exhibiting a fold–thrust and strike–slip with WMYB. Explaining the Himalayan alkaline mantle magmas, which are connected with rare earth mineralization derived from the remelting of the subducting Yangtze slab, is difficult.

In contrast to the frontal conclusion, alkaline magma formed in the subduction environment. However, this was not the case. These parallel suture belts in WMYB show bidirectional subduction in the Permian–Triassic period, and only the LCS show eastward subduction in the Tethys Ocean (Zhu Qinwen et al., 1998). The systematic compositional zonation of incompatible trace element abundances, Sr-Nd-Pb, and the melt segregation depths confirms the increase in potassic igneous rocks from SW to NE with increasing distance from the western margin of the Yangtze craton (Wang et al., 2001; Gou et al., 2005). Therefore, in the Himalayan period, with the continuous overriding and crustal shortening, an eastward old slab may exist under the WMYB. Previous studies found that the Himalayan carbonatite–alkalic complex in the Panzhihua–Xichang region has an extremely high $(^{87}Sr/^{86}Sr)_i$ of 0.706578–0.706925 and a relatively low $(^{143}Nd/^{144}Nd)_i$ of 0.512390–0.512423 (Tian Shihong, 2005), consistent with the Himalayan alkaline rocks in the Jinshajiang zone. The zircon Hf isotopes of the Lizhuang nordmarkite show that the $\varepsilon_{Hf}(t)$ values vary from −0.41 to 1.89, with an average of 0.66, and that the zircon model age varies from 989 Ma to 1145 Ma, with an average of 1067 Ma, which is similar to the granites in the LCS (early Triassic collision type) (Wang Baodi et al., 2011).

Therefore, the Lizhuang nordmarkite requires an early subduction and later strike–slip-related petrogenetic model (Fig. 11). The mantle lithosphere beneath the western part of the Yangtze craton in the Mesozoic was affected by a strike–slip network of a fluid-derived metasomatic vein. As a result of the strike–slip faulting and heat flow vector from the asthenosphere, the previously enriched mantle wedge beneath the western part of the Yangtze craton preferentially underwent decompressional melting, which triggered the formation of alkali magmas.

5.4 Constraints on the genesis of ore deposit

Previous studies pointed out that the Lizhuang REE

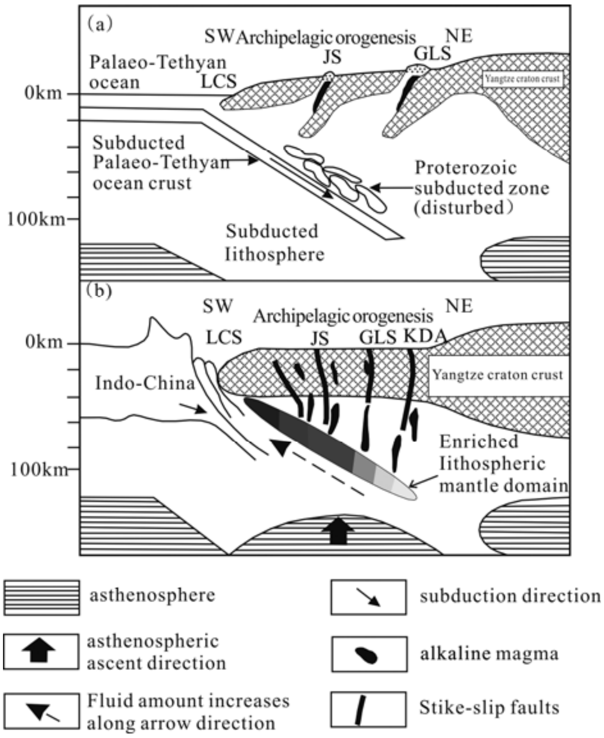

Fig. 11. Schematic representation of the model for alkaline magma genesis in the WSYP (modified from Guo, 2005).

deposit is located in the Jinping orogenic belt of the WMYB. The U-Pb dating with a weighted mean of 28.57±0.61 Ma, being consistent with the REE metallogenic age (28.5Ma) (Tian Shihong et al., 2008), is later than the orogenesis of Jinping mountain (about 224–213 Ma) (Yan Quanren et al., 2006) but close to the period of the large-scale strike–slip in the EMTP (Hou Zengqian et al., 2008). Therefore, based on the forming model of the Lizhuang nordmarkite, described as the early subduction and the later strike–slip faulting, the forming progress of REE deposit may be described as a result of the strike–slip and heat flow from the asthenosphere. The old slab under the WMYB preferentially underwent decompressional melting and triggered the formation of alkali magmas. With the rise and emplacement of alkali magmas along the strike–slip fault because of immiscibility, the REE-rich ore-forming fluids were segregated from the alkali magmas. With the subsequent intrusion and crystallization, the specific ore-fluids finally formed the REE ores in the shallow fault zone. Therefore, the formation model of the REE deposit in the area should be reconsidered as a special slip type and not as an orogenic type as previously proposed.

6 Conclusion

(1) The crystallization age of the zircons (28.57±0.61 Ma) indicates that the formation of the Lizhuang nordmarkite is a separate event from the subduction/collision between the Yangtze Block and the Tibetan plateau. The Lizhuang nordmarkite is derived from an enriched mantle beneath the western part of the Yangtze craton, which originated from the remelting of the Palaeo–Tethys subducting slab.

(2) The formation of the enriched mantle was controlled by transfer faults, which indicate that the partial melting of the Palaeo–Tethys subducting slab, which formed an enriched mantle beneath the deep lithosphere, maybe connected with the extensional strain brought on by transfer faults.

(3) The ore genesis of these rare earth deposits in the WMYB can be described as the mantle-derived magma melting the Palaeo–Tethys subducting slab because of the Yanshanian collision orogeny and the Himalayan strike–slip fault, intruding along the strike–slip fault, causing immiscibility in a deep place, and separating from the enriched REE fluid. The enriched REE fluid uplifted and crystallized following the magma, finally forming a special type of REE deposit called strike–slip type REE deposits.

Acknowledgments

Zircon cathode luminescence image analysis and LA-ICP-MS zircon U-Pb dating were conducted in the Chinese Academy of Geological Sciences Institute of Mineral Resources. We are grateful to Dr. Hou Kejun for his kind support.

Manuscript received Febr. 23, 2017
accepted Aug. 10, 2017
edited by Liu Lian

References

Andersen, T., 2002. Correction of common lead in U-Pb analyses that do not report ^{204}Pb. *Chemical Geology*, 192(1–2): 59–79.

Bell, K., and Simonetti, A., 1996. Carbonatite magmatism and plume activity: implications from the Nd, Pb and Sr isotope systematic of Oldoinyo Lengai. *Journal of Petrology*, 37: 1321–1339.

Belousova, E.A., Griffin, W.L., O'Reilly, S.Y., and Fisher, N.L., 2002. Igneous zircon: Trace element composition as an indicator of source type, *Contributions to Mineralogy and Petrology,* 143: 602–622.

Belousova, E.A., Griffin, W.L., and Pearson, N.J., 1998. Trace element composition and cathodoluminescence properties of southern African kimberlitic zircons. *Mineralogical Magazine,* 62(3): 355–366.

Chen Jun and Wang Henian, 2004. *Geochemistry*. Beijing: Science press, 1–410 (in Chinese).

Claiborne, L.L., Miller, C.F., and Wooden, J.L., 2010. Trace element composition of igneous zircon: a thermal and compositional record of the accumulation and evolution of a large silicic batholith, Spirit Mountain, Nevada. *Contributions to Mineralogy and Petrology,* 160(4): 511–531.

Cong Bolin, 1988. *Formation and Evolution of the Panxi Paleo-rift*. Beijing: Science Press. 427 (in Chinese with English abstract).

Elhlou, S., Belousova, E., Griffin, W.L., Pearson, N.J., and O'Reilly, S.Y., 2006. Trace element and isotopic composition of GJ-red zircon standard by laser ablation. *Geochimica et Cosmochimica Acta*, 70(18) (suppl): A158.

Fu, B., Mernagh, T.P, Kita, N.T., Kemp, A.I.S, and Valley, J.W., 2009. Distinguishing magmatic zircon from hydrothermal zircon: A case study from the gidginbung high-sulphidation Au-Ag-(Cu) deposit, SE Australia. *Chemical Geology,* 259: 131–142.

Griffin, W.L., Wang, X., Jachson, S.E., Pearson, S.E.O., Reilly, S.Y., Xu, X.S., and Zhou, X.M., 2002. Zircon chemistry and Manma genesis, SE China: In-situ analysis of Hf isotopes, Tonglu and igneous complexes. *Lithos*, 61: 273–269.

Grimes, C.B., John, B.E., and Kelemen, P.B., 2007. Trace element chemistry of zircon from oceanic crust: A method for distinguishing detrital zircon provenance. *Geology*, 35(7): 643–646.

Guo Zhengfu, Jan Hertogen, Liu Jiaqi, Paul Pasteels, Ariel Boven, Lea Punzalan, He Huaiyu, Luo Xiangjun and Zhang Wenhua, 2005. Potassic magmatism in western Sichuan and Yunnan Provinces, SE Tibet, China: petrological and geochemical constrains on petrogenesis. *Journal of petrology*, 16(1): 33–73.

Helena, C., Brites, M., Pedro, P.S., and Joana, A., 2014. Zircon crystal morphology and internal structures as a tool for magma sources: Examples from northern Portugal variscan biotite-rich granite plutons. *Comptes Rendus Geoscience*, 346: 233–243.

Hoskin, P.W.O., and Schaltegger U., 2003. The composition of zircon and igneous and metamorphic petrogenesis. *Reviews in mineralogy and geochemistry*, 53: 27–55.

Hoskin, P.W.O., Kinny, P.D., Wyborn, D., and Chappell, B.W., 2000. Identifying accessory mineral saturation furing differentiation in granitoid magmas: an integrated approach. *Journal of Petrology,* 41: 1365–1396. Hoskin P W O. 2005. Trace-element composition of hydrothermal zircon and the alteration of Hadean zircon from the Jack Hills, Autralia. *Geochim. Cosmochim. Acta,* 69: 637–648.

Hou Kejun, Li Yanhe and Tian Yourong, 2009. In situ U-Pb zircon dating using laser ablation-multiion counting-ICP-MS. *Mineral deposit,* 28(4): 481–492 (in Chinese with English abstract).

Hou Kejun, Li Yanhe, Zou Tianren, Qu Xiaoming, Shi Yuruo and Xie Guiqing, 2007. Laser ablation-MC-ICP-MS technique for Hf istope microanalysis of zircon and its geological applications. *Acta Petrologica Sinica*, 23(10): 2595–2604 (in Chinese with English abstract).

Hou Zengqian, Pan Guitang, Wang Anjian, Mo Xuanxue, Tian Shihong, Sun Xiaoming, Ding Lin, Wang Erqi, Gao Yongfeng, Xie Yuling, Zeng Pusheng, Qin Kezhang, Xu Jifeng, Qu Xiaoming, Yang Zhiming, Yang Zhusen, Fei Hongcai, Meng Xiangjin and Li Zhenqing, 2006. Metallogenesis in Tibetan collisional orogenic belt: Ⅱ. Mineralization in late-collisional transformation setting. *Mineral deposits,* 25(5): 521–543 (in Chinese with English abstract).

Hou Zengqian, Tian Shihong, Xie Yuling, Yang Zhusen, Yuan Zhongxin, Yin Shuping, Yi Longsheng, Fei Hongcai, Zou Tianren, Bai Ge and Li Xiaoyun, 2009. The Himalayan Mianning-Dechang REE belt associated with carbonatite-alkaline complexes, eastern Indo-Asian collision zone, SW China. *Ore Geology Reviews*, 36: 65–89.

Hou Zengqian, Tian Shihong, Xie Yuling, Yuan Zhongxin, Yang Zhusen, Yin Shuping, Fei Hongcai, Zou Tianren, Li Xiaoyu and Yang Zhiming, 2008. Mianning-Dechang Himalayan REE belt associated with carbonatite-alkalic complex in eastern Indo-Asia collision zone, southwest China: Geological characteristics of REE deposits and a possible metallogenic model. *Mineral Deposits*, 27(2): 145–176 (in Chinese with English abstract).

Lei Weiyan, Shi Guanghai and Liu Yingxin, 2013. Research progress on trace element characteristics of zircons of different origins. *Earth Science Frontiers,* 20(4): 273–284 (in Chinese with English abstract).

Li Huan, Koich Watanabe and Kotaro Yonezu, 2014. Zircon morphology, geochronology and trace element geochemistry of the granites from the Huangshaping polymetallic deposit, South China: Implications for the magmatic evolution and mineralization processes. *Ore Geology Reviews,* 60: 14–35.

Li Xianhua, Liang Xirong, Sun Min, Liu Ying and Tu Xianglin, 2000. Geochronology and geochemistry of single-grain zircon: Simultaneous in-situ analysis of U-Pb age and trace elements by LAM-ICP-MS. *European Journal of Mineralogy*, 12(5): 1015–1024.

Liu Yan, Hou Zengqian, Tian Shihong, Zhang Qichao, Zhu Zhimin and Liu Jianhui, 2015. Zircon U-Pb ages of the Mianning-Dechang syenites, Sichuan Province, southwestern China: Constraints on the giant REE mineralization belt and its regional geological setting. *Ore Geology Reviews*, 64: 554–568.

Liu Yongsheng, Hu Zhaochu, Gao Shan, Gunther Detlef, Xu Juan, Gao Changgui and Chen Haihong, 2008. In situ analysis of major and trace elements of anhydrous minerals by LA-ICP-MS without applying an internal standard. *Chemical Geology,* 257(1–2): 34–43.

Ludwig, K.R., 2003. *User's Manual for Isotopic 3.0: A Geochronological Toolkit for Microsoft Excel*. Berkeley: Berkeley Geochronology Center. Special Publication. No.4, 25–32.

Luo Yaonan, Yu Rulong, Hou Liwei, Lai Shaomin, Fu Deming, Chen Maoxun, Fu Xiaofang, Rao Rongbiao and Zhou Shishu,1998. *Longmenshan - Jinpingshan Intracontinental Orogenic Belt*. Chengdu: Sichuan Science and Technology Publishing House, 171 (in Chinese with English abstract).

Ma Yanping, Ling Yiping and Xu Guowei, 2007. The application of zircon study in geological science. *Jiangxi Nonferrous Metals*. 21(4): 4–7 (in Chinese with English abstract).

Miao Yikun, Ren Zude and Chen Xiaoyun, 1986. Tectonic environment and tectonic development of Panxi rift in Sichuan. *Earth Science-Journal of Wuhan College of Geology*, 11(6): 631–637 (in Chinese with English abstract).

Mitchell, A.H.G., and Garson, M.S., 1981. *Mineral deposits and global tectonic setting*. Academic press, 43–86.

Nardi, L.V.S., Formoso, M.L.L., Jarvis, K., Oliveira, L., Bastos, N.A.C., and Fontana, E., 2012. REE, Y, Nb, U and Th contents and tetrad effect in zircon from a magmatic-hydrothermal F-rich sys of Sn-rare metal-cryolite mineralized granites in the Pitinga Mine, Amazonia, Brazil. *Journal of South American Earth Sciences,* 33(1): 34–42.

Peter, D.K., and Roland, M., 2003. Lu-Hf and Sm-Nd isotope systems in zircon. *Reviews in Mineralogy and Geochemistry*, 53(1): 327–341.

Pettke, T., Audetat, A., Schaltegger U., and Heinrich, C.A., 2005. Magmatic-to-hydrothermal crystallization in the W-Sn mineralized Mole Granite (NSW, Australia)-Part Ⅱ: evolving zircon and thorite trace element chemistry, *Chemical Geology,* 220: 191–213.

Pu Guangping, 2001. The evolution history of rare earth elements mineralization and major features of Himalayan REE deposits in the Panzhihua-Xichang area, Sichuan. In: *Study on Himalayan endogenic mineralization*. Beijing: Seismological Press, 104–116 (in Chinese with English abstract).

Song Biao, Zhang Yuhai, Wan Yusheng and Jian Ping, 2002. Mount making and procedure of the SHRIMP dating. *Geological review*, 48(Supp): 26–30 (in Chinese with English abstract).

Taylor, S.R., and MeLennan, S.M., 1985. *The continental crust: Its composition and evolution: an examination of the geochemical record preserved in sedimentary rocks*. Oxford: Blackwell Oxford, 1–312.

Tian Shihong, Hou Zengqian, Yang Zhusen, Chen Wen, Yang Zhiming, Yuan Zhongxin, Xie Yuling, Fei Hongcai, Yin Shuping, Liu Yingchao, Li Zheng and Li Xiaoyu, 2008. Geochronology of REE deposits in Mianning-Dechang REE metallogenic belt: constraints on duration of hydrothermal activities and tectonic model for carbonatite-alkalic complexes in southwestern Sichuan. *Mineral Deposits*, 27(2): 177–187 (in Chinese with English abstract).

Tian Shihong, 2005. *The Himalayan Mianxi REE metallogenic belt on the Eastern Margin of the Qinghai-Tibet Plateau: Geology, Geochemistry and Geodynamics of the Mineralization*. Beijing: Institute of Mineral Resources, CAGS (Ph. D thesis): 1–151 (in Chinese with English abstract).

Wang Baodi, Wang Liquan, Qiangba Zhaxi, Zeng Qinggao, Zhang Wanping, Wang Dongbing and Cheng Wanhua, 2011. Early Triassic collision of northern Lancangjiang suture: Geochronological, geochemical and Hf isotope evidences from the granitic gneiss in Leiwuqi area, East Tibet. *Acta Petrologica Sinica,* 27(9): 2752–2762 (in Chinese with English abstract).

Wang Denghong, Yang Jianmin, Yan Shenghao, Chen Yuchuan and Xu Jue, 2002. Dynamics of the REE mineralization in maoniuping area Sichuan province: isotopic geochemistry of carbonatites. *Journal of Chengdu University of Technology*, 29(5): 539–544 (in Chinese with English abstract).

Wang Denghong, Yang Jianmin, Yan Shenghao, Xu Jue, Chen Yuchuan, Pu Guangping and Luo Yaonan, 2001. A special orogenic type rare element deposit in Maoniuping, Sichuan, China: Geology and geochemistry. *Resource Geology*, 51(3): 177–188.

Wang Jianghai, Yin An, Mark Harrison T., Marty Grove, Zhang Yuquan and Xie Guanghong, 2001. A tectonic model for Cenozoic igneous activities in the eastern Indo-Asian collision zone. *Earth and Planetary Science Letters*, 188: 123–133.

Wang Xiaofeng, Metcalfe I, Jian Ping, He Longqing and Wang Chuanshan, 2000. The Jinshajiang-Ailaoshan suture zone, China: tectonostratigraphy, age evolution. *Jounal of Asian Earth Sciences*, 18(6): 675–690.

Wu Yuanbao and Zheng Yongfei, 2004a. Genesis of zircon and its constraints on interpretation of U-Pb dating. *Chinese Science Bulletin,* 49(16): 1589–1604 (in Chinese).

Wu Yuanbao, Chen Daogong, Zheng Yongfei, Xia Qunke and Tu Xianglin, 2004b. Trace element geochemistry of zircons in migmatitic genesis at Manshuihe, North Dabieshan and its geological implications. *Acta Petrological Sinica*, 20 (5): 1141–1150 (in Chinese with English abstract).

Xie Liewen, Zhang Yanbin, Zhang Huihuang, Sun Jinfeng and Wu Fuyuan, 2008. In situ simultaneous determination of trace elements, U-Pb and Lu-Hf istopes in zircon and baddeleyite. *Chinese Science Bulletin,* 53(2): 220–228 (in Chinese).

Xu Cheng, Campbell I H, Kynicky J, Allen C M, Chen Yanjing, Huang Zhilong and Qi Liang, 2008. Comparison of the Daluxiang and Maoniuping carbonatitic REE deposits with Bayan Obo REE deposit, China. *Lithos*, 106:12–24.

Xu Cheng, Huang Longzhi, Liu Chongqiang, Qi Liang, Li wengbo and Guang Tao, 2002. The geochemistry of carbonatites of maoniuping REE deposit in Sichuan province. *Science in China* (Series D), 32(8): 635–643 (in Chinese).

Xu Zhiqin, Li Huaqi, Hou Liwei, Fu Xiaofang, Chen Wen, Zeng Lingseng, Cai Zhihui and Chen Fangyuan, 2007. Uplift of the Longmen-Jinping orogenic belt along the eastern margin of the Qinghai-Tibet plateau: large-scale detachment faulting and extrusion mechanism. *Geological Bulletin of China*, 26(10): 1262–1276 (in Chinese with English abstract).

Xu Zhiqin, Wang Qin, Li Zhonghai, Li Huaqi, Cai Zhihui, Liang Fenghua. Dong Hanwen, Cao Hui, Chen Xijie, Huang Xuemeng, Wu Chan and Xu Cuiping, 2016. Indo-Asian collision: tectonic transition from compression to strike slip. *Acta Geologica Sinica,* 90(1): 1–23 (in Chinese with English abstract).

Yan Quanren, Wang Zongqi, Liu Shuwen, Shi Yuruo, Li Qiugeng, Yan Zhen, Wang Tao, Wang Jianguo, Zhang Dehui and Zhang Hongyun, 2006. Eastern margin of the Tibetan plateau: a window to probe the complex geological history from the Proterozoic to the Cenozoic revealed by SHRIMP analyses. *Acta Geologica Sinica,* 80(9): 1285–1294 (in Chinese with English abstract).

Yin, A., and Mark, H.T., 2000. Geologic evolution of the Himalayan-Tibetan orogen. *Annual Review of Earth and Planetary Sciences*, 28: 211–280.

Yin Zhengxin, Yuan Yajuan, Liu Baofeng, Cai Zhourong, Zhang Hao, Huang Qiangtai, Xia Bin, Zhong Yun, Xia Zhongyu, Shi Xiaolong and Guan Yao, 2015. Zircon U-Pb geochronology and Hf isotopic constraints on Petrogenesis of Plagiogranite from the cuomuqu ophiolite, Bangong lake area, north Tibet. *Acta Geologica Sinica* (English Edition), 89(2): 481–440.

Yu Anguang and Guo Jianqiang, 1998. Tectonic framework on the western margin of the Yangtze platform. *Regional Geology of China*. 34(7): 613–621 (in Chinese with English abstract).

Yu Yushuai, Yang Zhusen, Duo Ji, Hou Zengqian, Tian Shihong, Meng Xiangjin, Liu Hongfei, Zhang Jinshu, Wang Haiping and Liu Yingchao, 2011. Age and petrogenesis of magmatic rocks from Jiaduobule skarn Fe-Cu deposit in Tibet: evidence from zircon SHRIMP U-Pb dating, Hf isotope and REE. *Mineral deposits,* 30(3): 420–434 (in Chinese with English abstract).

Yuan Yajuan, Yin Zhengxin, Liu Weiliang, Huang Qiangtai, Li Jianfeng, Liu Hongfei, Wan Zhifeng, Cai Zhourong and Xia Bin, 2015. Tectonic evolution of the Meso-Tethys in the western segment of Bangonghu-Nujiang suture zone: insights from geochemistry and geochronology of the Lagkor Tso Ophiolite. *Acta Geologica Sinica* (English Edition), 89(2): 369–388.

Yuan Zhongxing, Shi Zeming, Bai Ge, Wu Chengyu, Chi Ruan and Li Xiaoyu, 1995. *The Maoniuping rare earth ore deposit, Mianling County, Sichuan Province*. Beijing: Seismological press, 1–21.

Zhang Benren and Fu Jiamo, 2005. *Advances in Geochemistry*. Beijing: Chemical Industry Press, 1–437 (in Chinese).

Zhang Yueqiao, Chen Wen and Yang Nong, 2004. $^{40}Ar/^{39}Ar$ dating of shear deformation of the Xianshuihe fault zone in west Sichuan and its tectonic significance. *Science in China* (Series D), 47(9): 794–803.

Zhang Yunxiang, Lu Yaonan and Yang Chongxi, 1988. *The Panxi rift*. Beijing: Geological Publishing House, 224–270 (in Chinese).

Zhou Jianxiong and Cheng Zhengyu, 2007. *Study on cathodoluminescence of zircon by electron probe*. University of Electronic Science and Technology Press, 1–349 (in Chinese).

Zhou Jiayun, Zheng Rongcai, Shen Bing, Zhu Zhimin, Chen Jiabiao, Liu Feiyan and Wen Huaguo, 2007. Geochemiscal characteristics of the host intrusion of Muluo REE Deposit in Mianning, Sichuan Province, and their tectonic significance. *Journal of mineralogy and Petrology*, 27(1): 83–89 (in Chinese with English abstract).

Zhu Qinwen, Zhang Shuangquan and Tan Jin, 1998. Geochemical evidence of volcanic rocks for determining the south Lancangjiang suture zone. *Acta Petrological et Mineralogica,* 17(4): 298–307 (in Chinese with English abstract).

About the first author

ZHOU Jiayun, male; born in 1973 in Dayi County, Sichuan Province; doctor; professorate Senior Engineer of Institute of Multipurpose Utilization of Mineral Resources, Chinese Academy of Geological Sciences. He is now interested in the study on deposit geochemistry. Email: zhszjy@aliyun.com; phone: 028-85592028, 13608211820.